

Organic semiconducting thin film growth on an organic substrate: 3,4,9,10-perylenetetracarboxylic dianhydride on a monolayer of decanethiol self-assembled on Au(111)

M. C. Gerstenberg

*Princeton Materials Institute, Princeton University, Princeton, New Jersey 08544
and Chemistry Department, Princeton University, Princeton, New Jersey 08544*

F. Schreiber

*Institut für Theoretische und Angewandte Physik, Universität Stuttgart, 70550 Stuttgart, Germany
and Max-Planck Institut für Metallforschung, 70569 Stuttgart, Germany*

T. Y. B. Leung

*Princeton Materials Institute, Princeton University, Princeton, New Jersey 08544
and Chemistry Department, Princeton University, Princeton, New Jersey 08544*

G. Bracco*

Chemistry Department and Princeton Materials Institute, Princeton University, Princeton, New Jersey 08544

S. R. Forrest[†]

*Princeton Materials Institute, Princeton University, Princeton, New Jersey 08544
and Department of Electrical Engineering, Center for Photonics and Optoelectronic Materials (POEM),
Princeton University, Princeton, New Jersey 08544*

G. Scoles[†]

*Princeton Materials Institute, Princeton University, Princeton, New Jersey 08544
and Chemistry Department, Princeton University, Princeton, New Jersey 08544*

(Received 8 September 1999)

We use surface x-ray diffraction to study the structure of organic-organic heterojunctions grown by organic molecular-beam deposition. In particular, we study films of 3,4,9,10-perylenetetracarboxylic dianhydride (PTCDA) grown on a decanethiol self-assembled monolayer (SAM) on a Au(111) surface. The deposition of several (≈ 16) monolayers of PTCDA results in unstrained crystalline films whose (012) lattice planes are rotated 21.6° with respect to the $\langle 11\bar{2} \rangle$ Au azimuthal direction. This alignment, which is different from that of PTCDA on the bare Au(111) surface, is most likely caused by the corrugation of the SAM surface [with the $c(4 \times 2)$ superlattice of the $\sqrt{3} \times \sqrt{3}R30^\circ$ unit cell]. The SAM structure was found to be unaltered by the presence of the PTCDA overlayer. In addition, the heterogeneous PTCDA/SAM/Au structure, acting as an x-ray interferometer with the SAM as a spacer, allows for the precise determination of the SAM thickness.

I. INTRODUCTION

Thin films of relatively large organic molecules (i.e., with atomic masses in the range from 200 to 1000 amu) are potentially useful for electronic and optoelectronic applications such as organic light emitting devices, solar cells, field effect transistors, and sensors.^{1,2} In particular, the less severe lattice matching condition between adsorbate and substrate, which applies to organic film growth, has expanded the choice of materials available for the design of thin films. However, a high density of defects leading to a low-carrier mobility has been a limiting factor in the practical utilization of this type of material. The optimum conditions leading to ordered thin-film growth have been sought from the study of monolayers on inorganic substrates using traditional ultrahigh vacuum (UHV) characterization techniques. It has been found that the strength of the interaction with the substrate, the substrate symmetry, and the growth conditions are key factors in determining film structure and morphology.¹

Planar π -stacking organic molecules such as (oligo)thiophene,^{3,4} naphthalene, perylene, and their derivatives,¹ have been shown to be excellent model compounds for studying the growth and optoelectronic properties of organic semiconducting thin films on metal and semiconductor substrates. The interlayer bonding by the relatively flexible van der Waals (vdW) interaction results in ordered films over extended distances without a high density of strain-induced defects. One of the archetypal molecules belonging to this group is 3,4,9,10-perylenetetracarboxylic dianhydride (PTCDA) (see Fig. 1), which has been grown on various substrates such as highly oriented pyrolytic graphite (HOPG), MoS₂, Ag(111), Ag(110), Ni(111), Ge(100), Cu(100), Au(111), GaAs(100), Se-terminated GaAs, and the alkali halides (see Refs. 1 and 2 and references therein).

One of the factors that determine the structure of the first monolayer of PTCDA is the strength of the interaction with the substrate. On Ag(111), PTCDA monolayers form a commensurate base-centered rectangular unit cell (“herringbone

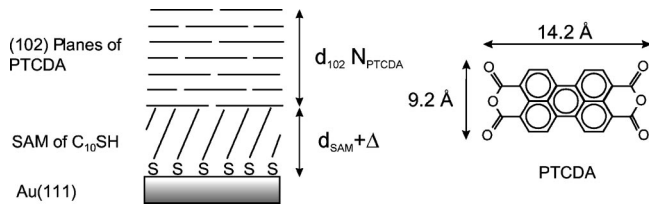


FIG. 1. Left: A schematic of the PTCDA/decanethiol/Au(111) double layer structure. In the figure, d_{102} denotes the distance between (102) PTCDA planes, N_{PTCDA} the number of (102) planes, and $d_{SAM} + \Delta$ the vertical distance between the lowest lying (102) PTCDA plane and the outermost Au(111) lattice plane (see Sec. III A). Right: The molecular structure of PTCDA with the dimensions calculated from the van der Waals radii of the constituents.

structure”), which is observed on most inorganic substrates,¹ whereas on the stronger binding Ag(110), a commensurate almost square unit cell (“brick stone structure”) was found.^{2,5} For more weakly binding (“inert”) substrates, e.g., HOPG and MoS₂, the substrate has only a weak influence on the PTCDA overlayer, and long-range order is achieved due to the dominance of intermolecular forces between PTCDA molecules. In this case, the substrate only serves as a two-dimensional (2D) base for the organic layer. The condition for incommensurate yet ordered growth on such substrates was suggested to be due to a large intralayer stiffness compared with a small interlayer shear stress.⁶

Depending on the growth conditions, the structure formed in the first and second layers can be maintained or relaxed towards the bulk in thicker films. When the organic thin film is grown under nonequilibrium conditions, i.e., high deposition rates and low substrate temperatures,^{1,7} the organic thin-film structure may be significantly distorted from the bulk. On Au(111), PTCDA forms a highly strained, incommensurate structure with mesa-like morphology in this regime with no apparent strain relief as the thickness of the film is increased.⁷ By comparison, equilibrium growth (i.e., low deposition rates and high surface temperatures) results in a relaxed three-dimensional island morphology after the first few monolayers. On HOPG, which has a weaker interaction with PTCDA than Au(111), PTCDA was observed to form a long-range and orientationally ordered incommensurate structure under non-equilibrium conditions.^{8–11}

While most studies have focused on the growth of organic films on inorganic substrates, little is known about thin film growth of organic molecules on an organic substrate. This is largely due to the difficulties in producing well-characterized and reproducible organic surfaces. In a four-layer alternating structure of 20-Å PTCDA and 20-Å 3,4,7,8-naphthalenetetracarboxylic dianhydride (NTCDA), each layer was found to be crystalline with its own well-defined surface unit cell.¹² Other studies have centered on PTCDA on copper phthalocyanine (CuPc), where it was found that PTCDA did not have crystalline order within the layers when grown on 20-Å CuPc on HOPG,¹² whereas PTCDA deposited on 2 monolayers (ML) of CuPc/Cu(100) indicated the presence of crystallinity with a structural change of PTCDA from a base centered to a rectangular unit cell after several monolayers.¹³ Even though these studies, based on reflection high-energy and low-energy electron diffraction (RHEED and LEED, respectively), have indicated that it is possible to

grow crystalline organic films on organic substrates, to our knowledge no detailed study of the structural properties of organic-organic heterointerfaces has been performed to date. Nevertheless, many fully organic heterostructure devices such as light-emitting devices are currently being exploited for commercial applications, making their full structural understanding imperative to future rapid advancements in the technology. Furthermore, the substrate surface can determine the properties of the deposited organic thin film via the introduction of an interfacial organic buffer layer of variable structure and electronic properties. Understanding the layer structure represents a first step in our ability to control the properties (both electronic and optical) of such interfaces.¹⁴ This understanding has been slow to develop due to the difficulty in structurally characterizing organic monolayer systems. However, due to their stability and relative ease of preparation, a few systems have been thoroughly studied, among which are monolayers of the *n*-alkanethiols [CH₃(CH₂)_{*n*-1}SH or C_{*n*}SH] self-assembled on Au(111). At present, these self-assembled molecules (SAM’s) can be grown on Au(111) with reproducible coverage and structure,^{15,16} and therefore offer a good choice for a well-characterized organic substrate.

Here we use grazing incidence x-ray diffraction (GIXD) to study ultrahigh vacuum deposited PTCDA on the *organic* surface of a decanethiol SAM (see Fig. 1). We find that it is possible to grow highly oriented and unstrained thin films of stacked organic molecules on these surfaces without altering the SAM ordering.

II. EXPERIMENT

The samples were grown *in situ* by molecular-beam deposition in a UHV chamber¹⁷ operated at a base pressure of $\sim 10^{-9}$ Torr. The chamber, equipped with a beryllium window for grazing incidence x-ray diffraction, mounts directly onto a Huber four-circle diffractometer situated at beam line X10B at the National Synchrotron Light Source at Brookhaven National Laboratory. The instrumental resolution was set by the variable aperture of the slits in front of the detector. We define the momentum transfer as $\mathbf{Q} = \mathbf{k}_f - \mathbf{k}_i$ with $Q = (4\pi/\lambda)\sin(2\theta/2)$, where \mathbf{k}_f and \mathbf{k}_i are the scattered and incident wave vectors of the x-rays at a wavelength of $\lambda = 1.130$ Å, and 2θ is the scattering angle. The momentum transfer (\mathbf{Q}) is resolved into its components parallel (Q_{\parallel}) and perpendicular (Q_{\perp}) to the surface. For the zeroth-order rod (wide-angle specular reflectivity) measurements, the resolution was $\Delta Q_z = 0.007$ Å⁻¹, whereas for the in-plane measurements, $\Delta Q_{\parallel} = 0.025$ Å⁻¹ and $\Delta Q_z = 0.037$ Å⁻¹.

A rectangular coordinate system (\mathbf{a}, \mathbf{b}) is chosen on the Au(111) substrate surface with \mathbf{a} along the next nearest-neighbor direction, $\langle 11\bar{2} \rangle$, and \mathbf{b} along the nearest-neighbor direction, $\langle 1\bar{1}0 \rangle$, with the lengths of the lattice vectors equal to 4.997 and 8.66 Å, respectively.^{17–19} The (1,1) and the (0.5,2) diffraction peaks refer to the $(\sqrt{3} \times \sqrt{3})R30^\circ$ hexagonal ordering of the hydrocarbon chains of the SAM and the $c(4\sqrt{3} \times 2\sqrt{3})R30^\circ$ superstructure, respectively. The latter is typically denoted $c(4 \times 2)$. For the PTCDA film, we adopt the notation previously obtained for the bulk structure.^{20,21}

Prior to deposition, the Au(111) single-crystal substrate was cleaned by repeated sputtering/annealing cycles until the $(23\times\sqrt{3})$ surface reconstruction of Au(111) (Ref. 22) remained stable for more than 30 min.

A full-coverage SAM was deposited on the gold crystal by back filling the UHV chamber to a pressure of $\sim 3\times 10^{-5}$ Torr with decanethiol ($C_{10}SH$) vapor from a leak valve source attached to the chamber. The coverage was monitored during growth by taking azimuthal scans of the (1,1) decanethiol diffraction peak, the integrated intensity of which is proportional to the coverage.^{16,23} The approximate domain size of the SAM was determined from the azimuthal full-width-at-half-maximum of the (1,1) hexagonal diffraction peak. To further increase the domain size,¹⁸ the SAM was annealed at $\sim 80^\circ\text{C}$ for several minutes, which should eliminate any vacancy islands.²⁴

Commercially available PTCDA was purified in three consecutive cycles by gradient sublimation¹² before loading it into the effusion cell positioned 200 mm from the substrate. The source was thoroughly degassed at elevated temperatures ($\sim 300^\circ\text{C}$) before deposition to avoid impurities and moisture that lead to the generation of defects during growth.¹² The rate of thin-film deposition was controlled by the temperature of the resistively heated Knudsen cell. The growth conditions were chosen to correspond to the non-equilibrium regime for PTCDA on Au(111) (Ref. 7) with a growth rate of ~ 8 ML/min and a substrate temperature of 21°C .

After the growth of the PTCDA layer, both the (1,1) and the (0.5,2) SAM peaks showed no apparent changes in shape and intensity indicating that the SAM domain size remained constant [see Figs. 2(a) and 2(b)]. Furthermore, Fig. 2(c) shows the (1,1) Bragg rod, which gives information on the tilt angle and direction of the hydrocarbon chains with respect to the substrate. It is evident that the (1,1) rod was not altered by the PTCDA deposition, from which we infer that the structure of the SAM is unaffected by the PTCDA overlayer.

III. RESULTS

A. Out-of-plane structure

Figure 3 shows three wide scan x-ray diffraction patterns of the peak intensity along the ridge of the zeroth-order rod obtained for the clean Au(111) surface (triangles), after deposition of the SAM (circles), and after deposition of ~ 16 ML (see below Table I) of PTCDA (diamonds). The background has been subtracted from the data. In Fig. 3(a), the Au(111) lattice planes separated by $d_{111}^{\text{Au}}=2.355$ Å give rise to the diffraction peak at $Q=2.668$ Å⁻¹ on the crystal truncation rod. It is evident from Fig. 3(b) that deposition of the decanethiol SAM layer gives rise to slight additional interference (Kiessig) fringes with a series of local minima appearing at $Q=0.79\pm 0.03$, 1.20 ± 0.01 , and 1.58 ± 0.02 Å⁻¹ with an average separation between minima of $\delta Q=0.39\pm 0.02$ Å⁻¹. Thus, the thickness of the SAM (d_{SAM}) can be roughly estimated as $d_{\text{SAM}}=2\pi/\delta Q\approx 16$ Å.

Deposition of PTCDA gives rise to diffraction features centered around $Q_{102}=1.927\pm 0.002$ Å⁻¹ [see Fig. 3(c)], which are assigned to the (102) reflection.^{7,25,26} Figure 4

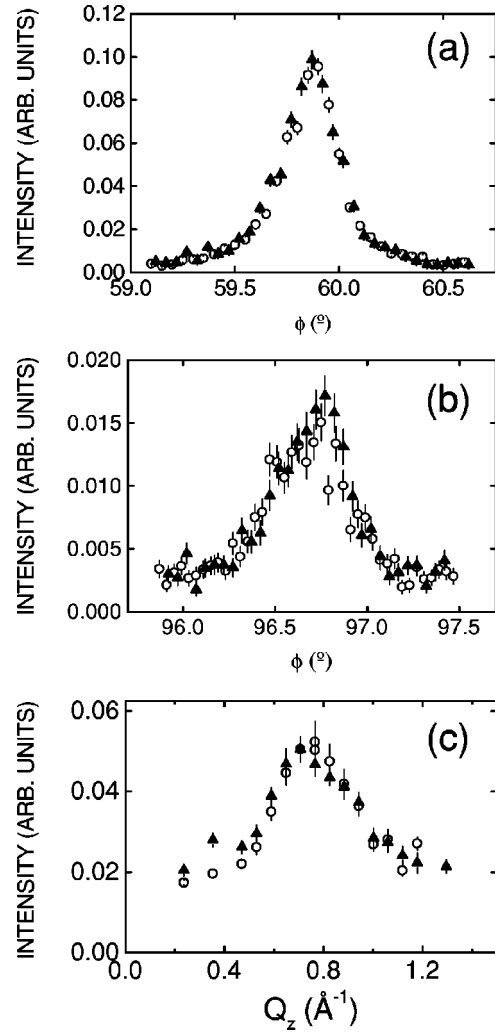


FIG. 2. Diffraction from the SAM ordering before (open circle) and after (filled triangle) PTCDA deposition, providing evidence for an unaltered SAM. Each set of scans are in the same arbitrary units. (a): The (1,1) ‘hexagonal’ peak, (b): The (0.5,2) superlattice peak, and (c): The (1,1) rod (raw data, i.e., not corrected for experimental resolution).

shows the rocking curve of the (102) peak centered at $\theta_0=2\theta/2$, indicating that Q_{102} is parallel to the surface normal. Hence, the PTCDA film grows preferentially with the (102) planes parallel to the Au substrate, consistent with previous observations for the growth of PTCDA on most inorganic substrates.¹

Apart from the PTCDA-related peaks, fringes can be clearly discerned at Q less than 1.8 Å⁻¹ in Fig. 3(c). The positions of the corresponding minima, $Q=0.90\pm 0.02$, 1.32 ± 0.01 , and 1.73 ± 0.02 Å⁻¹, are linearly displaced from the fringe minima in the SAM/Au(111) pattern as indicated by the vertical lines and arrows, but have about the same spacing δQ . Even though fringes (Laue oscillations) relating to the total thickness of the PTCDA layer ($\Delta Q=0.12$ Å⁻¹) should be discernible with the instrumental resolution, none are observed in Fig. 3(c) likely because of the film roughness.

At the (204) PTCDA peak ($Q=2Q_{102}=3.85$ Å⁻¹) destructive interference between the beams reflected from the PTCDA layers and the SAM is observed (see Fig. 5). In effect, the SAM acts similarly to the spacer in an optical

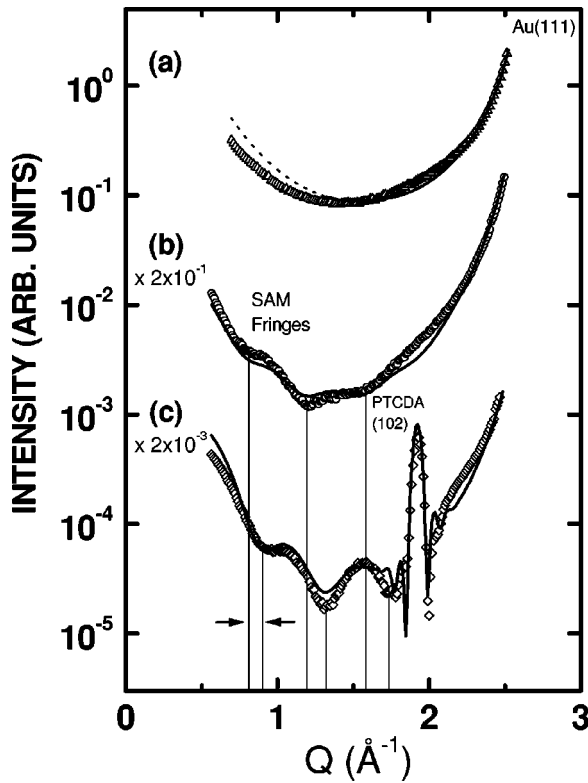


FIG. 3. The zeroth order rod measured for (a): Au(111), (b): SAM/Au(111), and (c): 16 ML PTCDA/decanethiol SAM/Au(111). The solid lines mark model fits as described in the text and the dashed line the region where the corrections to the model are difficult to assess due to the experimental conditions used. The errorbars are on the size of the points and are omitted for clarity.

etalon. The “dip” due to the destructive interference at the (204) PTCDA peak is highly sensitive to the thickness of the SAM and can therefore be used as a precise tool for its determination.

We have used a simple phenomenological approach to fit the x-ray diffraction patterns to obtain structural information from the zeroth-order rods. While our approach contains the essential contributions, some subtleties have not been included in the present treatment, which may limit its absolute

TABLE I. Characterization parameters obtained from the interference model of the PTCDA/SAM/Au(111) heterostructure for the model fits shown in Figs. 3 and 5. In the table β (σ_{rms}) denotes the Au roughness parameter, d_{SAM} the SAM thickness, Δ the difference between the gold-PTCDA gap and the SAM thickness, d_{102} the interplanar distance of the PTCDA layers, N_{PTCDA} the number of PTCDA layers, and $\sigma_{p'}$ and $\sigma_{p''}$ the roughnesses associated with the PTCDA layers.

Parameter	
β (σ_{rms})	0.46 ± 0.02 (3.0 ± 0.2 \AA)
$d_{\text{SAM}} + \Delta$	16.9 ± 0.2 \AA
Δ	4.9 ± 0.2 \AA
d_{102}	3.24 ± 0.03 \AA
N_{PTCDA}	16 ± 3
$\sigma_{p'}$	7 ± 2 \AA
$\sigma_{p''}$	0.36 ± 0.03 \AA

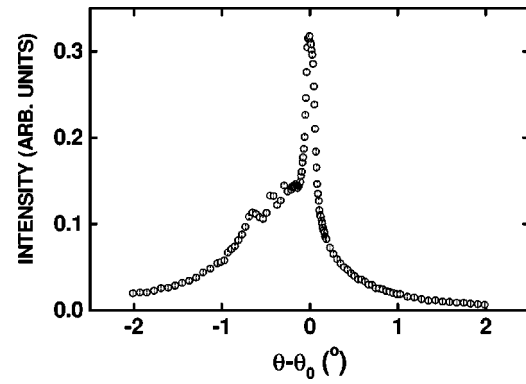


FIG. 4. Rocking curve of the (102) PTCDA peak showing that the (102) planes stack along the Au substrate normal. The specular condition is fulfilled when $\theta = \theta_0$, where $\theta_0 = 2\theta/2$ and 2θ is the scattering angle.

accuracy.²⁷ For simplicity, we neglect possible relaxation effects of the topmost Au layers. Whereas this has some impact on the overall shape of the rod, it does not significantly affect the pronounced interference effects, which are the focus of our analysis. The diffraction amplitude obtained for the bare Au substrate [Fig. 3(a)] is modeled as a crystal truncation rod (CTR) with amplitude:²⁸

$$A_{\text{Au}}(Q) = f_{\text{Au}} \frac{1 - \beta}{1 - \exp(iQd_{111}^{\text{Au}}) - \beta \exp(-iQd_{111}^{\text{Au}}) + \beta}, \quad (1)$$

where the roughness parameter β (with $0 < \beta < 1$) is the fractional occupancy of the outermost Au surface. The form factor for a layer of Au atoms, i.e., the electron density per area of a Au layer ($10.96 \text{ e}/\text{\AA}^2$) times the normalized form factor for Au,²⁹ is included in f_{Au} since all layers have the same atomic density.³⁰ The scattered x-ray intensity is $I \sim c_{\text{corr}} |A_{\text{Au}}|^2$, where the factor $c_{\text{corr}} \propto 1/Q^2$ due to the Lorentz factor and active area corrections. Since in our experiment we intended to make use of the full incident photon flux, the entrance slits were not very tight. Therefore, at low angles ($Q < 1.6 \text{ \AA}^{-1}$), where the sample does not intersect the whole incident x-ray beam, $c_{\text{corr}} \propto 1/Q$. However, Fig. 3(a) shows this correction only partially accounts for the loss in

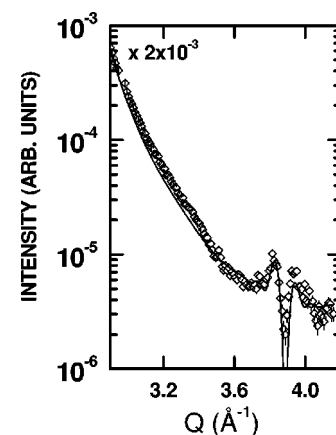


FIG. 5. The destructive interference at the (204) PTCDA Bragg peak. The solid line is the model described in the text with parameters listed in Table I.

intensity at low Q . Consequently, we have disregarded this region (dashed line) in the fitting of the rod.

The value of β is related to the root-mean-square (rms) roughness by

$$\sigma_{\text{rms}} = \frac{\beta^{1/2}}{1-\beta} d_{111}^{\text{Au}}. \quad (2)$$

For the Au CTR shown in Fig. 3(a), the best least-squares fit gives $\beta = 0.21 \pm 0.03$ (corresponding to $\sigma_{\text{rms}} = 1.4 \pm 0.2 \text{ \AA}$). We note, that σ_{rms} is much smaller than one would obtain in the small-angle reflectivity regime. In the wide-angle geometry with the resolution (coherence) used in the present experiment, we are mainly probing the roughness of the terraces, which is lower than the roughness from terrace to terrace.

The effect of the SAM on the zeroth-order rod is treated as the scattering obtained from a layer with homogeneous thickness and electron density. In the kinematical approximation, assuming sharp interfaces between the layers, the scattering amplitude can be calculated from³¹

$$A_{\text{SAM}}(Q) \sim i f_{\text{SAM}} \sin(Q d_{\text{SAM}}/2) e^{-iQ d_{\text{SAM}}/2} / Q, \quad (3)$$

where the form factor for the SAM layer, f_{SAM} , has been approximated as a constant electron density per area of a full coverage decanethiol monolayer (0.89 e/\AA^2) multiplied by the normalized form factor for a carbon atom.²⁹ By coherently adding the two contributions, i.e., $I \sim c_{\text{corr}} |A_{\text{SAM}} + A_{\text{Au}}|^2$,³² using $\beta = 0.44 \pm 0.02$ ($\sigma_{\text{rms}} = 2.8 \pm 0.2 \text{ \AA}$) and $d_{\text{SAM}} = 16.0 \pm 0.3 \text{ \AA}$, a reasonable fit to the data was obtained [solid line, Fig. 3(b)]. In the fitting we have used $c_{\text{corr}} \alpha 1/Q$ in order to obtain a value for the SAM thickness, d_{SAM} . However, this approach may yield a slightly increased β -value. Given the simplicity of the model (i.e., having a constant electron density for the SAM and having neglected possible relaxation effects of the Au surface), the value for the thickness is in reasonable agreement the estimate marked by the vertical lines in Fig. 3(b). The effective roughness of the Au surface appears to have increased after the deposition of the SAM, which is due to the presence of the sulfur atoms, smearing out the electron density profile.

The PTCDA slab is treated using a N -slit interference function

$$A_{\text{PTCDA}}(Q) = f_{\text{PTCDA}} \frac{1 - \exp(iQ d_{102} N_{\text{PTCDA}})}{1 - \exp(iQ d_{102})}, \quad (4)$$

where N_{PTCDA} and d_{102} denotes the number of lattice planes and the interplanar stacking distance of the PTCDA film, respectively. Also, f_{PTCDA} contains the form factor of a PTCDA layer, i.e., the normalized form factor of a PTCDA molecule multiplied by the electron density per area (1.680 e/\AA^2) assuming a base centered unit cell of dimensions $12.1 \text{ \AA} \times 19.9 \text{ \AA}$ (see Sec. III B).

From a comparison of the Kiessig fringes in the SAM/Au and the PTCDA/SAM/Au structures it is evident that the relative phase of the different scattering contributions influences the form of the rod, and therefore must be included in the model. Robinson *et al.* have previously analyzed the structure of the interface between a thin film of NiSi₂ and a Si(111) substrate,³⁰ which is conceptually analogous to the

PTCDA/SAM/Au(111) double layer assuming that the SAM has a vanishingly small electron density. The interface separation between the NiSi₂ layer and the Si(111) substrate was included as a phase factor in the calculation of the scattering amplitude, since the separation leads to a phase shift between waves diffracted from above and below this interface. Even though qualitative information could be obtained by modeling the SAM as a zero-density spacer on the PTCDA/SAM/Au(111) structure, this simple model, while fitting the PTCDA Bragg peak positions, does not provide an equally good fit elsewhere (i.e., at $Q < 1.5 \text{ \AA}^{-1}$). This is primarily due to the neglect of the nonzero SAM electron density. The (bulk) electron density of the SAM ($\rho_{\text{SAM}} = 0.29 \text{ e/\AA}^3$) is negligible with respect to the gold substrate ($\rho_{\text{Au}} = 4.65 \text{ e/\AA}^3$), but is comparable to the PTCDA electron density ($\rho_{\text{PTCDA}} = 0.51 \text{ e/\AA}^3$). Therefore, the SAM has to be taken into account in a more complete model for the total scattering intensity of the PTCDA/SAM/Au(111) structure, similar to buried layers in thin films.^{33,34} Consequently, we introduce a model,²⁷ where each layer is fully included in the scattering amplitude with an appropriate phase factor. Figures 3(c) and 5 (solid line) show the fit obtained using the more extended model, following:

$$\begin{aligned} A_{\text{tot}}(Q) = & A_{\text{PTCDA}}(Q, d_{102}, N_{\text{PTCDA}}) e^{-(Q - G_{h0(2h)})^2 \sigma_{P'}^2 - Q^2 \sigma_{P''}^2} \\ & + A_{\text{SAM}}(Q, d_{\text{SAM}}) e^{iQ[d_{102} N_{\text{PTCDA}} + (d_{\text{SAM}} + \Delta)/2]} \\ & + A_{\text{Au}}(Q, \beta, d_{111}^{\text{Au}}) e^{iQ[d_{102} N_{\text{PTCDA}} + (d_{\text{SAM}} + \Delta)]}, \end{aligned} \quad (5)$$

where $A_{\text{SAM}}(Q, d_{\text{SAM}}) = i f_{\text{SAM}} [\sin(Q d_{\text{SAM}}/2)/Q]$ is used for the SAM amplitude. To allow for structural inhomogeneities of the PTCDA layer, two roughness parameters have been included. The first rms roughness parameter ($\sigma_{P'}$) modifies the intensity of the side maxima of the N -slit interference function centered at $Q = G_{h0(2h)}$,³³ $h = 1, 2$, and accounts for fluctuations of the PTCDA layers on the order of a lattice constant, whereas the second factor ($\sigma_{P''}$) modifies the intensity of the PTCDA Bragg peaks arising from larger structural inhomogeneities such as steps on the PTCDA surface. Note that the model also includes a correction (Δ) to distinguish between the thicknesses obtained from the Kiessig fringes and the destructive interference at the (204) peak, respectively. The physical reason for this parameter is that in diffraction, where the thickness determination relies primarily on the position of the destructive interference at the (204) PTCDA peak, the thickness obtained is related to the vertical distance between the outermost Au layer and the lowest lying PTCDA layer, whereas the thickness inferred from the Kiessig fringes is the difference in vertical distance between the zeropoint of the derivative of the roughness profiles of the Au/SAM and the SAM/PTCDA interfaces. Therefore, the Kiessig fringes give an apparently smaller SAM thickness, d_{SAM} , than the gold-PTCDA thickness, $d_{\text{SAM}} + \Delta$, obtained by diffraction.

Finally, the intensity has been multiplied by $1/Q^2$, and has been convoluted with a Gaussian distribution with a standard deviation of $\sigma_{\text{res}} = 0.003 \text{ \AA}^{-1}$ to take into account the finite instrumental resolution. Similar to the Au rod, $c_{\text{corr}} \alpha 1/Q$ has been used near $Q < 1.6 \text{ \AA}^{-1}$. As seen in Figs. 3(c) and 5, the model adequately reproduces the features of the zeroth order

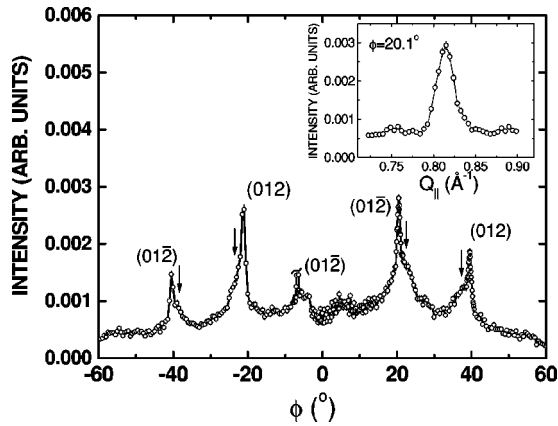


FIG. 6. Wide angle azimuthal scan through the (012) PTCDA Bragg peaks. The peaks are assigned assuming a base-centered rectangular unit cell. The inset shows a radial scan of the (01 $\bar{2}$) peak at $\phi = 20.1^\circ$. The symmetry equivalent peaks will appear slightly offset due to coupled motions of the four-circle spectrometer. The arrows mark the centers of the broader underlying peaks, whereas the tilted line indicates the cut off of a narrow spurious peak.

rod. Indeed, the intensity in the proximity of the second order Bragg reflection (Fig. 5) is reproduced well.

Table I provides a summary of the characterization parameters obtained by this fitting of the PTCDA/SAM/Au(111) structure. The measured gold-PTCDA thickness ($d_{\text{SAM}} + \Delta = 16.9 \pm 0.2 \text{ \AA}$) is consistent with the calculated value of $\sim 16.8 \text{ \AA}$, which is in turn based on a d_{SAM} value of 14.0 \AA (calculated from the full coverage structure as obtained by GIXD and x-ray standing wave methods³⁵ using standard bond angles and lengths³⁶) with the addition of the finite width of the lattice planes which can be roughly estimated as $(d_{102} + d_{\text{Au}})/2 = 2.8 \text{ \AA}$. The value found is also close to the ellipsometry estimate of $14.4 \pm 0.65 \text{ \AA}$,³⁷ which with the finite width of the lattice planes amounts to 17.2 \AA . The best fit for the Kiessig fringes was obtained for $\Delta = 4.9 \pm 0.2 \text{ \AA}$ resulting in a value d_{SAM} that deviates somewhat from the thickness obtained directly from the Kiessig fringes. Nevertheless, this Δ value is plausible considering that the sulfur layer of the SAM effectively acts on the density profile as a large surface roughness, which shifts the zeropoint of the differentiated density profile away from the outermost Au lattice plane.

Under the present experimental resolution conditions the relatively low effective roughness parameters (see Table I) refer to a small lateral length scale, i.e., essentially to the terraces themselves. Furthermore, for all sets of parameters, the PTCDA (102) lattice parameter is slightly increased from the nominal value of¹ $d_{102} = 3.21$ to $3.24 \pm 0.03 \text{ \AA}$. Note, that this apparent change in lattice parameter may be influenced by the interference between x-rays from the SAM and PTCDA layer at the PTCDA (102) peaks, the positions of which is slightly shifted.

B. In-plane structure

Figure 6 shows a wide azimuthal scan at $Q_{\parallel} = 0.813 \text{ \AA}^{-1}$ in close proximity to the (012) peak positions expected for an unstrained PTCDA lattice.^{20,21} The narrow components of the peaks ($\Delta\phi \approx 0.9^\circ$) show that PTCDA

grows in a preferred azimuthal orientation with respect to the underlying SAM. For the set of peaks shown, the optimized momentum transfer parallel to the surface is on average $Q_{\parallel}^{012} = (0.814 \pm 0.001) \text{ \AA}^{-1}$ with a resolution-limited radial width of $\Delta Q_{\parallel} = (0.025 \pm 0.001) \text{ \AA}^{-1}$. An intrinsic domain size (L_D) can be estimated from the azimuthal peak width using $L_D \approx 2\pi / (Q_{\parallel}^{012} \Delta\phi)$ from which we obtain $L_D \sim 500 \text{ \AA}$. For a 17 ML-thick PTCDA film deposited on Au(111) under identical conditions, the (012) reflections had azimuthal peak widths on the order of $\Delta\phi \approx 2^\circ$, which arose primarily from angular broadening and not the domain size.²⁵ In our case on the SAM, the angular broadening may contribute to the observed azimuthal width, making L_D a lower bound for the domain size. More importantly, by comparing the azimuthal peak widths, the PTCDA domains on the SAM are more azimuthally ordered than is found on Au(111). This behavior may be attributed to the weaker binding to the SAM substrate, where intermolecular forces between PTCDA molecules dominates. This results in a less distorted unit cell, allowing PTCDA molecules to more easily grow in an unstrained bulk structure.

Under the assumption that in the 2D planes PTCDA forms a base-centered rectangular unit cell (“herringbone structure”) typical of its crystal habit on weakly interacting substrates, the unit cell aspect ratio is related to the azimuthal separation of the (012) and the (01 $\bar{2}$) Bragg peaks. Denoting the 2D PTCDA lattice parameters as a_P and b_P , the peak separation is given by⁷

$$\Delta\phi = \phi_{012} - \phi_{01\bar{2}} = 2\arctan(2a_P/b_P). \quad (6)$$

The unit mesh in the (102) plane of the unstrained PTCDA lattice in the α -polymorph has the dimensions $(a_P, b_P) = (11.96 \text{ \AA}, 19.91 \text{ \AA})$,^{20,21} which gives a separation of $\Delta\phi = 100.5^\circ$ at an in-plane momentum transfer $Q_{\parallel} = 0.821 \text{ \AA}^{-1}$. When the sixfold symmetry of the SAM is taken into account, the (01 $\bar{2}$) peaks are separated from the (012) peak by 19.5° and 40.5° . Hence, we are able to assign the peaks at $\phi = -21.6^\circ$ and $\phi = 39.1^\circ$ to the (012) reflections, and $\phi = -40.9^\circ$ and $\phi = 20.1^\circ$ to the (01 $\bar{2}$) reflections, the reflections in each set being symmetry equivalent. Note that the β -polymorph gives corresponding values^{20,21} of 15.6° and 44.4° inconsistent with the peak separation. Assuming these assignments, PTCDA forms an unstrained rectangular surface structure with dimensions $12.1 \pm 0.1 \text{ \AA} \times 19.9 \pm 0.2 \text{ \AA}$, consistent with bulk values for the α polymorph.¹

IV. DISCUSSION AND CONCLUSION

Thin films of PTCDA approximately 16 ML thick were found to form an incommensurate ordered structure on the organic surface of a decanethiol SAM on Au(111). The “in-plane” domain size was typically larger than 500 \AA . Previous studies of this type of organic-organic interface have only been performed using techniques with limited resolution such as RHEED and LEED, eluding a full structural characterization.^{12,13} Here, by employing GIXD, both the in-plane and out-of-plane structures of PTCDA and the SAM were precisely measured. It was found that the SAM structure was unaffected by deposition of an overlayer of

PTCDA. As observed on many inorganic substrates, PTCDA was found to have the (102) stacking direction along the surface normal.^{1,38} The interfaces of this sandwich structure are sufficiently well defined to give rise to interference effects, most notably resulting in the destructive interference at the (204) PTCDA Bragg peak. From these data, we accurately determined the thickness of the SAM.

An important finding is the high lateral order observed for the PTCDA films deposited on the SAM. The (012) and (01 $\bar{2}$) peaks were found to have a narrower azimuthal width ($\Delta\phi=0.9^\circ$) than for PTCDA deposited on Au(111) ($\Delta\phi=2^\circ$). In addition, the only evidence for the presence of inequivalent domains of PTCDA, previously observed for PTCDA on Au(111),^{7,25,39} was a broad underlying component shifted approximately 0.8° from the (012) and (01 $\bar{2}$) peak positions (indicated by arrows, Fig. 6). In contrast to what happens on the SAM, the Au(111) surface interacts strongly with the PTCDA molecules creating a highly strained lattice that is maintained up to a thickness of at least 70 ML.⁷ The incommensurate PTCDA packing locks in to the Au(111) lattice, creating inequivalent domains due to several minima in the interface energy between the adsorbate and the substrate.^{6,39}

In our case, the hydrocarbon chains exert only a minor influence on the lateral packing of the PTCDA molecules through weak van der Waals interactions between the decanethiol -CH₃ endgroups and PTCDA. In this case, the PTCDA ordering is therefore likely to adopt the unstrained bulk structure. Nevertheless, the SAM structure still determines the orientation of the PTCDA overlayer as seen from the 21.6° rotation of the lattice with respect to the $\langle 11\bar{2} \rangle$ Au azimuthal direction. A similar effect has been observed for ‘end-capped’ quinquethiophene (EC5T) on Ag(111), where the interaction with the substrate did not force a commensurate structure, but nevertheless determined the relative orientation of the overlayer and substrate.³ A potential candidate leading to the PTCDA orientation is the corrugation of the hydrocarbon chains from the SAM structure which has been observed for *n*-alkanethiols on Au(111) with both low-energy atom diffraction⁴⁰ and scanning tunneling microscopy.⁴¹ The vertical displacement between hydrocarbon ends can be estimated to be ~ 0.5 Å based on recent structural findings by x-ray standing waves.³⁵ This results in lateral corrugation of the surface potential serving to orient the PTCDA even though the two lattices are incommensurate. The type of growth where film orientation is observed between weakly bonded, incommensurate layers has previously been termed ‘quasi epitaxy.’^{6,42}

Figure 7 shows schematically the PTCDA surface net on Au(111) (left) and on the decanethiol SAM (right). PTCDA has previously been observed^{39,43} to align along high-symmetry directions on some substrates.⁹ Even though the surface net of PTCDA on the SAM seems to be approximately (although not precisely) oriented along a high-

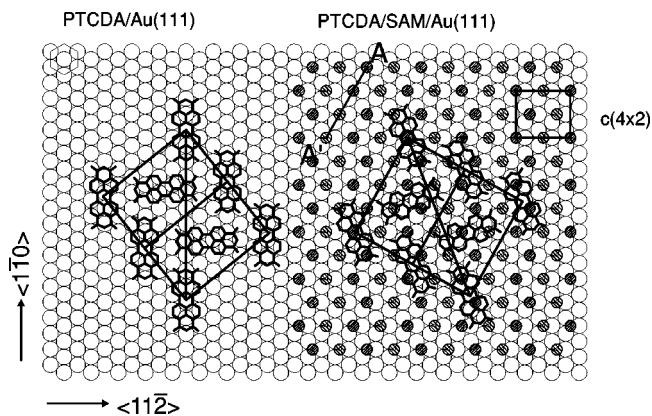


FIG. 7. A comparison of the unit cells found for PTCDA/Au(111) (Refs. 25 and 7) and PTCDA/SAM/Au(111). On the SAM the unit cell is rotated approximately 21.6° with respect to the one found on Au(111). The two types of cross-hatched circles denote thiol molecules that are distinct within the $c(4 \times 2)$ (shown in the top right-hand corner) unit mesh. The open circles denote the Au atoms of the substrate surface. The orientations of the surface nets relative to the substrate are tentative.

symmetry direction (line $A'-A$), it is not yet possible to unambiguously determine the position of the unit mesh of PTCDA relative to the SAM.

Finally, the modeling of the zeroth-order rod clearly shows that it is possible to describe the layering of organic-on-organic thin films with relatively simple models, despite the fact that organic thin films can have more complex structures than their inorganic counterparts.

In this study we have shown that it is possible to grow ordered layers of the large planar molecule PTCDA on the surface of an organic substrate of decanethiol. The self-assembled monolayers are found to be of sufficient quality to be used as substrate interface templates which initiate ordered growth of the PTCDA overlayer. The large variety of SAM end-groups offers unprecedented possibilities for the design of surface properties tailored to result in the growth of high quality organic thin films with a wide range of properties useful in modern optoelectronic devices.

ACKNOWLEDGMENTS

The authors wish to acknowledge the experimental assistance of B. Edinger and J. Krich and useful conversations with J. Libuda. F. Schreiber acknowledges useful discussions with N. Karl and B. Toperverg and generous support by H. Dosch. The GIXD measurements were performed at the National Synchrotron Light Source at Brookhaven National Laboratory which is supported by U.S. Department of Energy Contract No. DE-AC0276CH-00016. The work was carried out with the support of Princeton's MRSEC funded by the National Science Foundation, the Air Force Office of Scientific Research, the Max-Planck-Society, and the Deutsche Forschungsgemeinschaft.

*On leave from the Physics Department, University of Genova and INFN, Genova, Italy.

†Authors to whom correspondence should be addressed.

¹S.R. Forrest, Chem. Rev. **97**, 1793 (1997).

²E. Umbach, K. Glöckler, and M. Sokolowski, Surf. Sci. **402-404**, 20 (1998).

³A. Soukopp, K. Glöckler, P. Bäuerle, M. Sokolowski, and E. Umbach, Adv. Mater. **8**, 902 (1996).

- ⁴A. Soukopp, K. Glöckler, P. Kraft, S. Schmitt, M. Sokolowski, E. Umbach, E. Mena-Osteritz, P. Bäuerle, and E. Hädicke, *Phys. Rev. B* **58**, 13 882 (1998).
- ⁵C. Seidel, J. Poppensieker, and H. Fuchs, *Surf. Sci.* **408**, 223 (1998).
- ⁶S.R. Forrest and Y. Zhang, *Phys. Rev. B* **49**, 11 297 (1994).
- ⁷P. Fenter, F. Schreiber, L. Zhou, P. Eisenberger, and S.R. Forrest, *Phys. Rev. B* **56**, 3046 (1997).
- ⁸P.E. Burrows, Y. Zhang, E.I. Haskal, and S.R. Forrest, *Appl. Phys. Lett.* **61**, 2417 (1992).
- ⁹A. Hoshino, S. Isoda, H. Kurata, and T. Kobayashi, *J. Appl. Phys.* **76**, 4113 (1994).
- ¹⁰C. Ludwig, B. Gompf, J. Petersen, R. Strohmaier, and W. Eisenmenger, *Z. Phys. B: Condens. Matter* **93**, 365 (1994).
- ¹¹C. Kendrick, A. Kahn, and S.R. Forrest, *Appl. Surf. Sci.* **104/105**, 585 (1996).
- ¹²S.R. Forrest, P.E. Burrows, E.I. Haskal, and F.F. So, *Phys. Rev. B* **49**, 11 309 (1994).
- ¹³T.J. Schuerlein and N.R. Armstrong, *J. Vac. Sci. Technol. A* **12**, 1992 (1994).
- ¹⁴I.H. Campbell, J.D. Kress, R.L. Martin, and D.L. Smith, *Appl. Phys. Lett.* **71**, 3528 (1997).
- ¹⁵P. Fenter, in *Thin Films: Self-assembled Monolayers of Thiols*, edited by A. Ulman (Academic Press, 1998), Vol. 24.
- ¹⁶F. Schreiber, A. Eberhardt, T.Y.B. Leung, P. Schwartz, S.M. Wetterer, D.J. Lavrich, L. Berman, P. Fenter, P. Eisenberger, and G. Scoles, *Phys. Rev. B* **57**, 12 476 (1998).
- ¹⁷A. Eberhardt, Ph.D. thesis, Princeton University, 1997.
- ¹⁸P. Fenter, P. Eisenberger, and K.S. Liang, *Phys. Rev. Lett.* **70**, 2447 (1993).
- ¹⁹P. Fenter, A. Eberhardt, K.S. Liang, and P. Eisenberger, *J. Chem. Phys.* **106**, 1600 (1997).
- ²⁰A.J. Lovinger, S.R. Forrest, M.L. Kaplan, P.H. Schmidt, and T. Venkatesan, *J. Appl. Phys.* **55**, 476 (1984).
- ²¹M. Möbus, N. Karl, and T. Kobayashi, *J. Cryst. Growth* **116**, 495 (1992).
- ²²A.R. Sandy, S.G.J. Mochrie, D.M. Zehner, K.G. Huang, and D. Gibbs, *Phys. Rev. B* **43**, 4667 (1991).
- ²³A. Eberhardt, P. Fenter, and P. Eisenberger, *Appl. Surf. Sci.* **397**, L285 (1998).
- ²⁴G.E. Poirier, *Chem. Rev.* **97**, 1117 (1997).
- ²⁵P. Fenter, P.E. Burrows, P. Eisenberger, and S.R. Forrest, *J. Cryst. Growth* **152**, 65 (1995).
- ²⁶Typically, the average thickness of the film, L_p , can be estimated from the (102) peak width ($\Delta Q_{102} = 2\pi/L_p$) deconvoluted from the instrumental resolution. For the (102) peak shown in Fig. 3(c), this determination gives an equivalent of ~ 23 layers, however, this determination is quite rough since interference effects of the PTCDA/SAM/Au heterostructure may alter the width of the (102) peak.
- ²⁷A more complete treatment will be given in F. Schreiber, M. C. Gerstenberg, B. Toperverg, B. Edinger, S.R. Forrest, H. Dosch, and G. Scoles (unpublished).
- ²⁸I.K. Robinson, *Phys. Rev. B* **33**, 3830 (1986). We recognize that this treatment of the Au rod is an approximation, but the fit that it provides is adequate for our purposes in the measured Q -range. Furthermore, the measured data for the Au(111) rod does not validate the many parameter model as described by Sandy *et al.* (Ref. 22).
- ²⁹*International Tables for Crystallography* (Kluwer Academic, Dordrecht, 1992), Vols. B-C.
- ³⁰I.K. Robinson, R.T. Tung, and R. Feidenhans'l, *Phys. Rev. B* **38**, 3632 (1988).
- ³¹R. W. James, *The Optical Principles of the Diffraction of X-rays* (Cornell University Press, Ithaca, NY, 1965).
- ³²M. Schaub, C. Fakirov, A. Schmidt, G. Lieser, G. Wenz, G. Wegner, P.-A. Albouy, H. Wu, M.D. Foster, C. Majrzkak, and S. Satija, *Macromolecules* **28**, 1221 (1995).
- ³³J. Falta, D. Bahr, A. Hille, G. Materlik, and H.J. Osten, *Appl. Phys. Lett.* **71**, 3525 (1997).
- ³⁴U. Zimmerman, J.-P. Schlomka, M. Tolan, J. Stettner, W. Press, M. Hacke, and S. Mantl, *J. Appl. Phys.* **83**, 5823 (1998).
- ³⁵P. Fenter, F. Schreiber, L. Berman, G. Scoles, P. Eisenberger, and M.J. Bedzyk, *Surf. Sci.* **412-413**, 213 (1998); *ibid.* **425**, 138 (1999).
- ³⁶The thickness of the SAM was calculated assuming Au-S (Ref. 35), S-C, C-C, C-H bond lengths of 2.21 or 2.97 Å (gauche), 1.82, 1.54, 1.10, respectively, with C-S-C, C-C-C, and C-C-H bond angles of 112°, 110°, 110° respectively. The van der Waals radius of H, 1.2 Å, was included in the total hydrocarbon chain length. To obtain the SAM thickness the hydrocarbon chain is tilted¹⁹ 30° about the S atom and the Au-S interface was defined to be mid between the Au and S atom. All values were obtained from the *CRC Handbook of Chemistry and Physics*, 70th ed. (CRC Press, Boca Raton, FL, 1990) except otherwise marked.
- ³⁷W.J. Miller and N.L. Abbott, *Langmuir* **13**, 7106 (1997).
- ³⁸M. Möbus and N. Karl, *Thin Solid Films* **215**, 213 (1992).
- ³⁹T. Schmitz-Hübsch, T. Fritz, F. Sellam, R. Staub, and K. Leo, *Phys. Rev. B* **55**, 7972 (1997).
- ⁴⁰N. Camillone III, C.E.D. Chidsey, G.-Y. Liu, and G. Scoles, *J. Chem. Phys.* **98**, 3503 (1993).
- ⁴¹G.E. Poirier and M.J. Tarlov, *Langmuir* **10**, 2853 (1994).
- ⁴²F.F. So, S.R. Forrest, Y.Q. Shi, and W.H. Steier, *Appl. Phys. Lett.* **56**, 674 (1990).
- ⁴³C. E. Kendrick, Ph.D. thesis, Princeton University, 1997.